

CARBON NANOTUBE MECHANICS:

Molecular Simulations & Continuum Models for Carbon Nanotubes

Aaron Sears

advisor: R.C. Batra

Department of Engineering Science and Mechanics, MC 0219

Virginia Polytechnic Institute and State University

Blacksburg, VA. 24061

Abstract

To realize the incredible structural applications potential of carbon nanotubes, it is important to characterize their material response. Molecular simulations offer advantages over physical testing due to their cost effectiveness, versatility and precision. Two continuum models for single wall nanotubes (SWNT) were previously developed based on the results from molecular simulations using two different potentials. The continuum models have been found to predict both global and local responses for buckling well. Radial expansion and contraction simulations of double wall nanotubes confirmed that the assumption of isotropy of a nanotube wall response is accurate. The SWNT continuum models were used as the basis to model multi-wall nanotubes (MWNT). In continuum mechanics, the equivalence to the van der Waals forces is pressure. Using the results from the expansion/contraction simulations the pressure between two walls was defined as a function of the wall separation. A continuum model for MWNTs was developed using finite element (FE) analysis with shell elements for the walls and truss elements to substitute for pressure. The predictions from the FE models are compared to molecular simulations. Preliminary work on nanotube/polymer composite material is also presented.

Introduction

Since their discovery in 1991 by Iijima¹, both single wall and multi-wall carbon nanotubes (SWNTs & MWNTs) have become an active area of research. This is partly due to their having an extremely high specific strength and stiffness. These properties and their cylindrical shape allow for their potential applications in such diverse fields as fibrous reinforcement, atomic level piping and nanostructures. These structural applications of carbon nanotubes require that we ascertain their macroscopic properties.

In the simplest terms, carbon nanotubes can be thought of as rolled up, closed graphite sheets. This sheet can be rolled up at different discrete angles to create the SWNT which can be described by the

hexagonal base vectors $(a,b)^2$. Thus, an SWNT is a single, closed molecule with few to no atomic imperfections, and a hexagonal ring bonding structure similar to graphite. The molecular structure of an example SWNT is shown in Figure 1, next to a fullerene which Iijima was attempting to create when he discovered nanotubes. The ring bonding structure, specifically the hybridized sigma bonds (sp^2), imparts the impressive mechanical properties. Multi-walled nanotubes also exist, consisting of nested SWNTs 3.4 Å apart, which widen the range of tube properties and application possibilities.

Experimental studies have been performed to characterize nanotube materials. Due to the difficulty in performing these experiments, the scatter in the results is considerable and the stiffness of carbon nanotubes was found to lie between 0.5 - 4 TPa³⁻⁶. Stating these values underscores two common continuum assumptions, first that they are linear elastic materials and have a thickness corresponding to density of graphite ($t = 0.34$ nm). Naturally, with such poor resolution, the validity of these assumptions can not be checked with experiment.

Atomic simulations have proven to be a good vehicle for studying nanotube mechanical responses. Molecular mechanics has been used to obtain Young's moduli of 0.75 - 1.25 TPa⁷⁻¹⁰, using the same assumptions as detailed above. Molecular mechanics is a method of modeling the interatomic forces, including bonding and non-bonded forces, with simple polynomial and trigonometric expansions. This method was developed for the modeling of large molecules such as proteins and lends itself well to the study of nanotubes. The advantage of molecular mechanics is the precision with which tests can be performed. Not only can virtual tension tests be performed, but other tests such as torsion can be performed which are not yet feasible experimentally. The accuracy of these methods vary, but have been shown to predict moduli with the same precision as quantum mechanical methods¹¹⁻¹³. A listing of the experimental and molecular simulation modulus results from various studies can be found in last years review.

Motivation & Goals

Two popular continuum models exist for nanotubes. Both use molecular physical phenomena to define characteristic geometries. They also make simplifying assumptions that may or may not be appropriate. The resulting material models are simple and easily used in 'back of the envelope' style calculations. The most common, a thick walled tube with the density of graphite, is easily compared to macro-material properties and easily extended to incorporate MWNTs. While this model may work well for global responses, such as predicting the deflection of a MWNT cantilevered in bending, it cannot model the crimping behavior associated with high bending curvatures. The thin walled model is argued to be more valid for local instability modeling, such as shell wall buckling⁸. However, it was not tested for MWNTs or large aspect ratios. A membrane model was published that was verified for a large range of aspect ratios, walls and responses. However, it is a finite element model that has a complex derivation that requires either coding or acquisition of the authors' code for implementation¹⁴.

Therefore, a more comprehensive, yet simple, continuum material model for nanotubes is desired and is the goal of this work. It should be usable for the 'back of the envelope' calculations that are important for engineers when quick results are needed. It should also be robust enough to employ in more sensitive analysis that may require the use of more complex analyses. This model should be able to predict both local and global mechanical responses for various loads. For example, it should be able to predict crimping for long aspect ratio nanotubes in bending. It should also be applicable for SWNTs, MWNTs or as a base for composite material models. It was decided that the formulation of the model should adhere to common engineering practices for obtaining material properties. Thus, the approach taken here will mirror what an engineer would face when given a cylinder of an unknown metal alloy. This material may be directionally dependent or nonlinear. Therefore, a number of tests will be employed to determine which assumptions are acceptable, and to develop the model. The material properties will then be calculated using continuum mechanics relationships. This engineering approach also dictates that continuum assumptions will not be made from molecular physical phenomenon. Instead, they will be calculated or based solely on test results. Because of the exhaustive and precise experimental testing required, molecular simulations will be employed rather than physical testing.

The development of this model will be approached in three steps. First, a material model for a single wall

will be developed using molecular simulations of SWNTs. The molecular simulations will serve to mimic traditional material property tests. Simple tests, such as tension and torsion, will be used to build the continuum model. More complex tests, such as buckling, will be simulated to verify the application of the model to a wider range of responses. This work was accomplished in the previous year and only a short summary will be provided for completeness and help understanding the current work. Next, the model will be extended to MWNTs. Here the major test will be modeling the interwall interactions due to the van der Waal forces. The model should be robust enough to handle back of the envelope calculations or the complex responses requiring sensitive analysis of independent interwall movement. These models will also be developed and verified using molecular simulations. Lastly, a nanomechanics composite model will be developed which can predict the properties of composite materials for various nanotubes, the nanotube-polymer interactions and volume fractions.

Molecular Mechanics

The MM3 class II pair-wise potential with both higher-order expansions and cross-terms was used with type 2 (alkene) carbon atoms selected¹⁵. This potential is appropriate for carbon nanotubes due to the similarity between graphitic bonds in the nanotube and the aromatic protein structures for which potential was constructed. The Tersoff-Brenner (TB) potential, designed to study graphite, was also used¹⁶.

In summary, the procedure for simulating a mechanical test is multi-step process. First, it involves finding the minimum energy configuration of an unloaded nanotube, referred to as the relaxed structure or relaxed configuration. The deformed configuration is then estimated and displacement boundary conditions applied to appropriately selected atoms. With these atoms kept fixed, the remaining atoms are allowed to move freely till the minimum energy configuration is attained.

Summary of Previous Results

In the previous study the assumptions of linearity and directional dependence of SWNTs were studied. The equivalent continuum response of the MM3 and Tersoff-Brenner modeled nanotubes was found to be nonlinear. The axial stiffness of nanotubes with various (a,b) structures was found to vary linearly with strain. The effective Poisson's ratio and shear stiffness were also found to vary with strain. This effect was expected due to the form of the potential energy terms, especially the bond stretching term which had a higher energies in compression than tension. However, on closer analysis

of the MM3 potential energy terms the nonlinear response was caused by the interaction of all the terms rather than the dominance of just one.

The problem of finding a continuum cylindrical tube whose response to axial and torsional deformations is identical to that of a (16,0) SWNT is complicated by the fact that its response varies nonlinearly differently for different deformations. To simplify the problem, it was decided that the equivalent continuum tube is made of a linear elastic isotropic material with mean diameter equal to the diameter of the SWNT, wall thickness t , and moduli equal to those of the SWNT at zero strain. Thus,

$$E(0, t) = 2G(0, t)(1 + \nu(0)), \quad (1)$$

is the equation for the determination of the wall thickness t of the equivalent continuum tube. Knowing t , E and G can be computed.

The results are presented in Table 3 for the MM3 and the TB potentials. The wall thickness thus found equals 1.34 Å and 0.98 Å for the MM3 and the TB potentials respectively which differ from the common published values mentioned earlier. Had we used a wall thickness of 3.4 Å, then we would have obtained $E(0)$ to be 0.99 TPa and 0.89 TPa respectively for the MM3 and the TB potentials which compare favorably to the values reported in the literature.

Table 1. The wall thickness and elastic constants of a equivalent linear elastic continuum tubes.

potential	structure	thickness (Å)	E (TPa)	G (TPa)	ν
MM3	[16,0]	1.34	2.52	0.96	0.21
TB	[16,0]	0.98	3.10	0.81	0.26

The assumption of isotropy was checked through tests on various nanotube structures and the use of expansion and contraction models. Various (a,b) nanotube structures were tested and the results did not vary greatly. This means that neither the chiral (wrapping) angle nor curvature of the tube cause significant changes in the response, which indirectly infers that the tube is behaving isotropically. To apply circumferential strains to a nanotube wall, the van der Waals forces supplied by a separate wall were used. To apply compressive strains, the outer wall of a double wall nanotube is contracted to a new radius and held fixed. The resulting change in the wall separation distance increases the van der Waals forces between the walls and causes the inner wall to contract as well. From the results of several tests it was shown that the circumferential and axial stiffness were only 1%

different, which was considered a negligible difference. Thus, the assumption of isotropy is considered valid.

The SWNT continuum material model was validated by comparing predictions for bending and buckling against molecular simulations. Employing a simple Euler beam model for cantilever bending the continuum SWNT strain energy was found to match that of the simulation very well. The buckling of a SWNT was studied for tubes of different length to study both the local and global nanotube behavior. Long tubes will behave like columns and buckle as a unit, while at shorter lengths will undergo shell wall buckling behavior. Here the continuum tube was modeled using 8-node shell finite elements. The material model was found to predict the critical buckling strain of the nanotube for the whole length scale well as compared to the simulations.

MWNT Study

The material model found for SWNTs is a hollow tube geometry of ~ 1 Å thickness. The most natural extension of this model to a MWNT is to replace each wall with one cylinder. This results in concentrically nested cylinders with a gap between them. Thus two of the main objectives to developing an MWNT continuum model are; 1) verify that the SWNT model will work for MWNT walls, 2). determine the differences between SWNT and MWNT responses 3). define an interaction relationship between the walls.

Superposition and slip condition simulations were run which verified that the SWNT model does work for individual nanotube walls. The results are straightforward and not presented here.

Modeling van der Waals Forces

Some choices available to model the interaction between adjacent walls of a MWNT are: (i) lateral rigid connections between the two walls, (ii) filling the gap with a soft material, (iii) connecting atoms on two walls by trusses, (iv) assuming that a radial pressure acts on the walls. The lateral rigid connection essentially assumes a beam model where the MWNT acts as a single unit, which while simplifying also limits its range of use to global responses with large aspect ratios. The most direct, analogous continuum model for van der Waals forces is a pressure field and hence becomes the preferred method.

We postulate that van der Waals forces between the walls of a MWNT can be represented by a pressure field acting on the walls, where the pressure magnitude varies with the gap width and the radii of the walls. A similar assumption was made by Ru¹⁷ who did not find the pressure as a function of gap width. An expression for this pressure as a function was derived from MM

simulation results of the expansion/contraction models. This method is in contrast to other models developed in the literature by directly dispersing the discrete, van der Waals multibody expression to a continuum pressure field. The strain energy of deformation for several values of the separation distance between the two walls of a DWNT is expressed as strain energy per unit volume of the gap; its variation with the gap distance is exhibited in Figure 1. We note that it converges to $-1.1 \cdot 10^{-21} \text{ J}/\text{\AA}^3$. The following function,

$$W = 2\pi L \frac{K(b(s+r_i)+1)}{b^2(r_o^2-r_i^2)} \exp[-b(s-c)], \quad (2)$$

where $K = 9.5 \cdot 10^{-22} \text{ J}/\text{\AA}^3$, $b = 5.3 \text{ 1}/\text{\AA}$, $c = 3.52 \text{ \AA}$, and s is the wall separation distance, provides a good fit to the data of Figure 3.7 as indicated by the solid curve. This equation is valid for $2.6 \text{ \AA} < s < 3.4 \text{ \AA}$.

Assuming that the continuum structure is elastic, a pressure field between the adjoining walls of the two cylindrical tubes will deform them thereby altering the gap width. The strain energy of deformation can be expressed as a function of the gap width or equivalently of the gap strain defined in a way analogous to the axial strain. We recall that in MM simulations one wall of a DWNT is constrained from moving radially. We apply similar constraint to the continuum structure. Let $P_o(s)$ be the pressure acting on the inner surface of the outer continuum cylindrical tube. Then the strain energy of deformations of the continuum cylindrical tube, normalized by the gap volume, is given by,

$$W_{cont} = \frac{1}{\pi(r_o^2-r_i^2)L} \int_{s_o}^s 2\pi L(r_i+s)P_o(s)ds \quad (3)$$

where L is the length of the tube. Equating (2) and (3) and differentiating both sides with respect to s , we obtain

$$P_o(s) = K \exp[-b(s-c)], \quad (4)$$

that defines the relationship between the wall separation distance and the pressure between the walls.

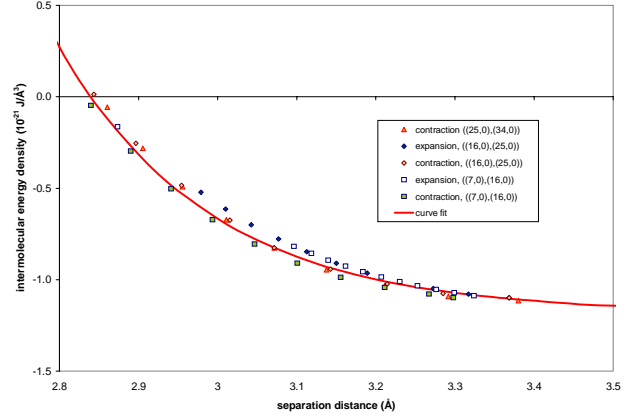


Figure 1. Results and fit of intermolecular energy density with respect to the wall separation distance for the radial expansion/contraction tests

Bending Deformations

Bending deformations of a $((7,0),(16,0))$ DWNT cantilever beam were analyzed with the MM3 potential. For a prescribed deflection of the free end, the Euler beam theory was used to estimate the deformed positions of atoms. The null displacement boundary conditions at the clamped edge were enforced by fixing positions of atoms of the outer wall $\sim 12 \text{ \AA}$ in from one end of the tube. The prescribed deflection at the other end was achieved by displacing three adjacent atoms $\sim 12 \text{ \AA}$ from the free end of the tube to minimize the wall indentation effects. With boundary conditions applied to atoms on the outer wall only, van der Waals forces act on atoms of the inner wall. The boundary conditions mimic an experimental set-up where only the outer wall can be tangibly loaded. For each prescribed deflection, axial positions of all atoms, including those with assigned deflections, were perturbed to find the minimum energy configuration of the bent tube.

The wall separation distance remained constant during the loading. Thus, rigid gap assumption between two concentric tubes is valid for global responses, thereby allowing the continuum model to be an Euler beam with a moment of inertia and cross sectional area equal to those of two concentric tubes. The deflected shape of the DWNT found by MM simulations agreed well with that given by the Euler beam theory. Strain energy results from the Euler beam theory applied to equivalent continuum tubes of varying cross section are shown in Figure 3.8 along with MM results. As with the buckling study for SWNTs from an earlier study, the thinner cross sections predict better results than the standard hollow cylinder model. The coefficient of deviation for each model versus the MM data at maximum deflection (31.7 \AA) is 1%, 2% and 10% for the thin shell, thick shell and no gap models,

respectively. Thus for beam bending where no kinking occurs a simple rigid gap, or Euler beam model, yields accurate results.

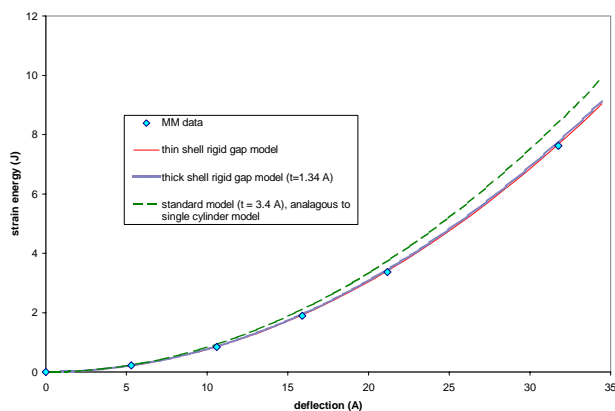


Figure 2. Comparison of the strain energy/atom versus the tip deflection as obtained by MM simulations and Euler-Bernoulli beam theory models

Buckling

Axially compressed buckling offers an interesting insight into the effect of the van der Waals forces. As the nanotube length changes the buckling response changes from a global to a local response. To better understand the mechanics of MWNT buckling, SWNT simulations were also run where the SWNTs share the (a,b) molecular structure with the walls of MWNTs that were studied. The four SWNTs studied were the (7,0), (16,0), (25,0), and (34,0) structures. These wall structures were chosen because they produce MWNTs with wall separation distances near the ideal distance of 3.4 Å.

In the Tinker molecular modeling program, boundary conditions are applied by fixing the location of desired atoms. Due to this feature, the clamped-clamped end conditions are the most straightforward and appropriate boundary condition to use for axial compression and buckling. The load is applied by moving each atom axially to affect the correct axial strain. To help induce buckling a sinusoidal wave perturbation is applied in a lateral direction to the locations of all the atoms. The onset of buckling was defined as when the maximum lateral deflection was either 1% of the length or 10% of the (16,0) wall radius. In these studies an automated combination between a truncated Newton and negative curvature method was used to minimize the potential energy.

The critical buckling strains of these tubes are plotted versus in Figure 3. The most relevant feature of this curve is that for long aspect ratios (length/diameter) the critical buckling strains of the MM simulations lay

on the Euler column buckling predictions. At shorter lengths the predictions deviate from the Euler predictions as the buckling modes transition to shell wall modes. As expected, the larger diameter tubes begin to transition at lower strain levels.

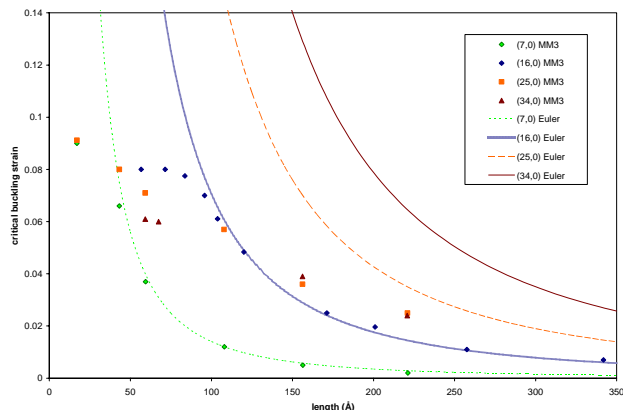


Figure 3. Critical buckling strains of SWNTs for differing lengths

The question that arises for MWNTs is, ‘will the MWNT buckle when the lowest critical buckling strain for an individual is reached, or will the walls tend to support each other?’ The question is best answered by viewing the results of double wall nanotube (DWNT) buckling simulations directly against the SWNTs that make up its walls. These results are shown for the ((7,0),(16,0)) and ((16,0),(25,0)) DWNTs in Figure 4.

The effect of the walls seems to be supportive. For long tubes, the MWNTs also tend to follow the Euler buckling predictions. If the walls did not support each other, we would expect the smaller diameter wall to buckle into a column mode near its SWNT buckling range and force the outer tube into that shape as well. Thus in that range supporting each other. For short tubes, the DWNT critical buckling strain seems to correspond with the inner wall. Since the outer tube should want to buckle before the inner, the inner wall is providing the resistance needed to delay buckling until it too buckles independently. The situation is less clear in the transition zone, where mixed column and crimping buckling modes are prevalent. There, the critical buckling strain is seen to deviate earlier from the Euler predictions than for its SWNT constituents.

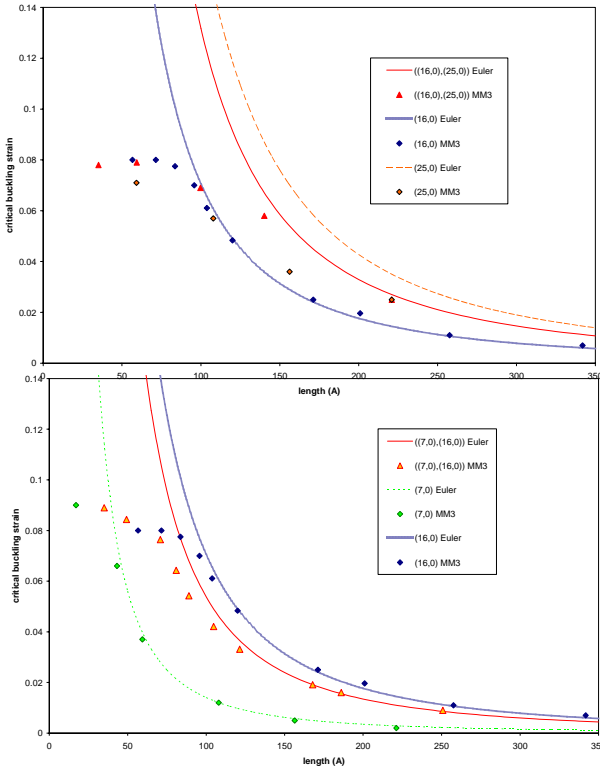


Figure 4. Critical buckling strains for DWNT and their constituent SWNT counterparts of differing lengths

A study of triple wall nanotubes (TWNT) is in the preliminary stages. Some interesting buckling modes have been found for a $((16,0),(25,0),(34,0))$ tube and are shown in Figure 5. For a moderate tube length of 156 \AA ($L/D \sim 6$) the outer tube is first seen to buckle into rippling pattern at 7% axial strain. As the strain level increases the middle tube is also forced into the rippling pattern at 7.9%. This phenomenon reinforces the hypothesis that the inner walls are effectively supporting the outer walls against buckling. From a different minimization starting point the same tube is seen to buckle into a fully developed shell wall buckling mode at 8% strain. These different responses highlight the non-uniqueness of the buckling response.

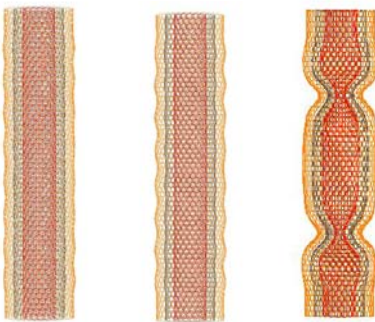


Figure 5. Example buckling models for a TWNT

Continuum MWNT Model Verification

The SWNT buckling and DWNT bending studies have shown that concentric tube based, rigid gap, Euler beam models can reproduce MM simulation data well. Therefore a MWNT buckling study should focus on local buckling effects and the transition between global and local effects. A $((16,0),(25,0))$ DWNT was found to be a good structure for studying these responses with MM, FE and Euler beam theory with traditional clamped-clamped boundary conditions. Both the MM and FE models utilized slight sinusoidal perturbations to help induce buckling events. The FE tube walls are modeled using 8-noded (6 DOF/node) shell elements with large strain and large rotation capabilities. Since the thick shell ($t = 1.34 \text{ \AA}$) yielded better results than the thin shell model across the responses, and the focus is now on modeling the tube interactions, only the thick shell is modeled here.

As outlined earlier, several options are available for modeling the van der Waals interactions. We use a combination of two types to study the buckling response. First, the lateral rigid connection is used to model Euler beam responses. Second, the pressure field developed in section 4 is used to study the interwall interactions. Unfortunately, with an objective being simplicity of approach, we used the readily available FE software package, Ansys, and a stable, convergent approach was not found.

Hence, a generalized truss model was implemented where the pressure field served as stress-strain curve to define a material system for the link elements making up the truss. Each node on one wall was attached to its adjacent mirror node on the other wall by a two node (3 DOF/node) link element. Due to the degree of freedom mismatch between the shell and link elements, a second set of coincident nodes were defined for the link elements and the displacement degrees of freedom coupled with the shell element nodes. An example of a DWNT FE model is shown in the inset of Figure 6. The link elements implemented a multi-linear elastic model and a cross sectional area which is $1/3$ of an inner wall shell element area, this gives 1:1 ratio of cylinder to link areas. Thus the multi-linearity of the link element may be pulled directly from the van der Waals pseudo-pressure (stress) versus strain curve. A second link material, arbitrarily determined, was also studied. This second material has zero stiffness around the equilibrium position, an increasingly stiffer response as the strain level is increased, and ends with a considerably stiffer modulus at strain levels of around 3%. This model, termed the 'loose arbitrary' model, was studied to see how the DWNT would respond when the walls were free to move independently within a

small range, thereby increasing the likelihood of small lateral shell deflections and buckling initiation.

The critical buckling strain results for the two DWNT buckling studies are shown in Figure 6. First the Euler column buckling predictions can be seen to match the MM results. The FE model also reproduces these results for the global buckling regime. Here both the pseudo-pressure and 'loose arbitrary' models were able to reproduce the global response. Both FE models were also able to follow the buckling initiation predictions into the transition zone. This shows that a range of van der Waals models may work reasonably well. In fact, the loose arbitrary model seems to perform slightly better, especially in the pure shell wall buckling modes. The pseudo-pressure model seems to predict slightly high buckling strains.

As with the SWNT buckling models, the DWNT FE mode shapes for the pure shell wall and column modes were good. However, the transition state, mixed modes were more difficult to capture. Given the simple, straightforward nature of the models, the results are considered to be adequate and quite promising.

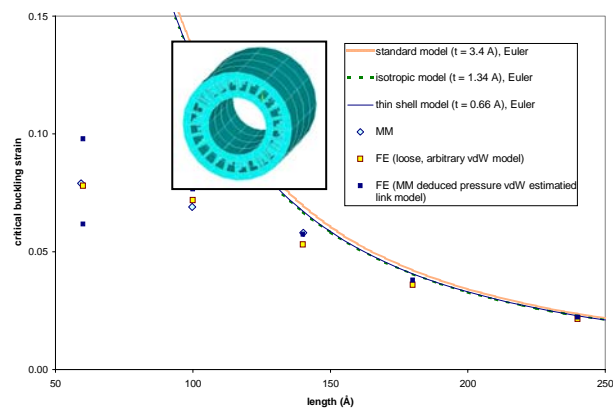


Figure 6. Critical buckling strains for FE models and molecular simulations of a DWNT for differing lengths (inset, cross section of the FE model)

Nanotube Composites

Nanotubes offer many striking characteristics that lead to the belief that they would be ideal fibrous reinforcement for composite materials. They have exceedingly high aspect ratios and stiffness and strength to weight ratios. Due to their nanoscale, which is on the same order as polymer chains, they also offer intriguing manufacturing possibilities. Unfortunately they have proven to be difficult to process, are very expensive and may not have good bonding characteristics. Most reinforcing fibers for polymer composites undergo chemical treatments to increase their bonding

characteristics with the polymer. Unfortunately, these techniques may also lead to detrimental changes in the crystal structure which imbues nanotubes with their high stiffness and strength.

A prime concern for engineers is to be able to predict the material properties of a composite before manufacturing the material. To accomplish this, nanomechanical models are needed which are similar to traditional laminar composite micromechanical models. To build a model, the nanotube-polymer interface must be better understood. Two main mechanisms have been proposed to transfer load from the matrix to the nanotube. The short range mechanism would be tangential load, shear stress transfer. This would occur via bonding (functionalization) or nonbonded forces. The non-bonded forces can be viewed as a type of traction or friction between the matrix and tube. This would be enhanced through local nanotube deformations which would be analogous to surface roughness. The long range mechanism is fiber-matrix entanglement. Both mechanisms will be studied here using two different analyses.

Nanotube size is on the same scale as the polymer chains, therefore, the short range mechanism can be studied using many of the same molecular mechanics tools that have been developed to elucidate nanotube mechanics. The polymer chains may be modeled using the same MM3 potential used earlier in the study. This allows for direct correlation between the composite mechanics and the nanotube mechanics. The first goal of the molecular simulations will be to find a simple nanotube-polymer interaction model. This model could be as simple as a friction coefficient or something more complex, depending on the results from the simulation. The effect of the polymer structure can be studied by controlling the input structure. Amorphous, crystalline and helically wrapped polymer structures can all be studied. A second goal will be to study the difference in the nanotube response between freestanding and polymer immersed nanotubes. For instance, the change in the critical buckling strains and modes due to the presence of the polymer matrix can be compared to those of the freestanding nanotube.

To study the larger scale interactions, where molecular simulations are impractical, continuum models may be used. The long range stress transfer mechanism is mechanical interlocking. This may be studied in conjunction with the affect of nanotube curvature. It has been shown that fiber waviness negatively affects the composite modulus, however, it is the curvature which causes the mechanical interlocking.

Virtual Pullout Test

The nanotube-polymer interface may be studied by a virtual pullout test. Here, a periodic nanotube is slid through the periodic box, along the nanotube axis. Cylindrical boundary conditions are implemented by fixing all atoms over a certain radius to be immovable. Inside this radius, all atoms are allowed to move freely. For a linear isotropic material, a linear shear deformation would be created for a perfectly bonded interface. Thus the molecular deformation field may be compared to the continuum field to define the polymer-nanotube interface. It is hoped that a strain transfer coefficient could be determined from these tests. It may be possible to tie the coefficient to nanotube surface roughness or polymer density. To the author's knowledge, no such study has been performed and such knowledge could be highly useful. The effect of slight nanotube curvature could also be studied by enforcing a sinusoidal deformation on the nanotube.

Nanomechanical Continuum Models

Great differences exist between nanotube fibers and traditional macroscale graphite fibers. It has been shown that issues of fiber waviness and load transfer across the material interfaces separate nanotube composites from traditional fiber composites. Despite these problems, nanotubes have been seen to improve on neat resin properties. It is natural to assume that standard micromechanics models, such as the rule of mixtures, may not accurately predict composite properties. Therefore, new nanomechanics models need to be developed to account for these differences. Finite element models offer advantages to elasticity models by making contact, friction and surface roughness issues more tractable. Two models, 2D and 3D, are proposed here which may capture both the long and short range stress transfer mechanisms. The major difference between these models and traditional FE composite micromechanics models is their ability to model the nanotube-polymer interface rather than assuming a perfect bond. They can also directly accommodate the continuum nanotube model developed in the earlier studies. These models may serve as a base for calculating effective fiber properties for nanotubes.

2D Long Range and Interface Model

An effective fiber model can be found in the literature that accounts for fiber waviness. However, the model did not account for the local fiber-matrix interface. It assumed a perfect bond existed at the interface, which may not be a good assumption. A 2D FE model is being developed that allows for slippage along the nanotube tangential direction. The nanotube is modeled as a beam whose initial shape is sinusoidal.

The polymer matrix elements are quadrilateral solids in plane stress with a finite thickness. Long range nanotube polymer entanglement is approximated through a combination of contact and overlapping elements. The polymer elements on either side of the nanotube are different than those in the rest of the polymer. Two elements are superposed on top of each other, defined by different but coincident nodes. The first element type has a reduced thickness and a free surface adjacent to the nanotube. Forces normal to the nanotube are transmitted to the nanotube by surface to surface contact elements. The second set of elements connect the polymer elements on one side of the beam with those on the other. These overlapping elements mitigate polymer separation from the beam, allowing the polymer to deform as unit. This is a natural assumption since polymer chains surround the nanotube, transferring stress and strain across the nanotube's plane. The thickness of the two element types sum to the polymer thickness in the rest of the polymer. The size of the adjacent polymer elements is very important to the transfer of load to the nanotube. The model is shown in Figure 4.1, with a close-up view of the adjacent elements highlighted on the right.

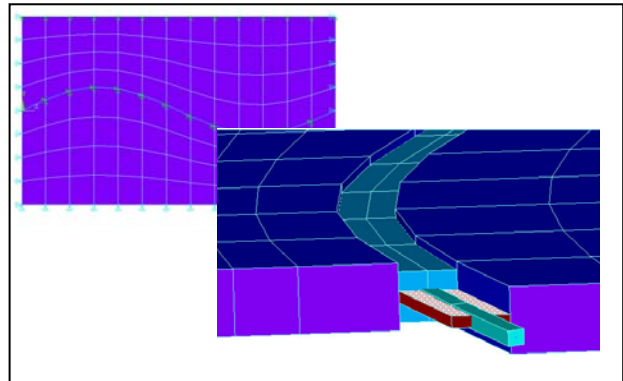


Figure 7. Views of the 2D continuum model with sinusoidal fiber and interface slippage

With this base model, tangential strain/stress transfer may be also be modeled by several methods. The current model is applicable for perfect bonding or free slip (no bonding). The interface stress transfer may be incorporated by expanding the contact model to include friction. Initial efforts with this have not proven fruitful. Constraint equations may also be used which tie the motion of one node to another by a linear equation. For both methods, the strain transfer could be modeled using the data from the MM virtual pull-through simulations. Preliminary results show that even for high amplitude sine wave shaped fibers, the free slip conditions reduce the fiber effectiveness severely. Thus, either some tangential stress transfer occurs, or

this model does not capture the long range fiber entanglement mechanism well.

3D FE Long Range and Interface Model

Another continuum model which may capture the long and short range interface stress transfer mechanisms is a 3D finite element model. Here, the nanotube is modeled as either solid brick elements or shell elements. The polymer elements would be modeled as brick elements. The interface could be handled in several ways. First, direct contact could be used, where the polymer elements may directly contact the fiber elements. The interface would thus be a perfect contact, free slip, constraint equation or friction model as discussed with the 2D model. Two advantages would be gained by going to 3D. First, the ambiguity of the adjacent element sizing would be nullified. Second, surface roughness could be added to model the non-uniform radial deformations seen in the molecular simulations, which may increase the stress transfer for the free-slip condition. Another method to model the interface would be to use truss elements similar to those used to model the interwall forces for MWNTs. Surface roughness may also be incorporated here.

Effective Fiber Determination

The results from the finite element models may be used to calculate an effective fiber for calculating the composite material properties. The effective fiber would be defined as the fiber properties of a straight fiber, with equivalent mass and volume fraction, whose interface has a perfect bond with the matrix and provides the composite material with the same properties as the wavy, slipping nanotube. The effective fiber coefficient would be defined as the ratio of the axial moduli of the effective fiber to that of the nanotube. This value would necessarily always be below one due to the degrading effects of waviness and imperfect bonding. The effective fiber allows traditional micromechanics to be used to predict composite properties. Since a range of nanotube curvatures is found in manufactured composites it will be necessary to define different effective fibers for differing curvatures. Parametric studies of wave amplitude would define different effective fiber coefficients for a specific interface. The effective fibers can be related to the fiber curvatures seen for nanotube composites in TEM images. A distribution of the fiber curvatures can also be estimated by the TEM images. Thus the distribution of effective fibers may be estimated and the composite material properties may be calculated using a statistical approach.

References

- ¹ S. Iijima, Nature **354**, 56-58 (1991).
- ² C. T. White, D. H. Robertson, and J. W. Mintmire, Physical Review B **47**, 5485-5488 (1992).
- ³ M. M. J. Treacy, T. W. Ebbesen, and J. M. Gibson, Nature **381**, 678-680 (1996).
- ⁴ E. W. Wong, P. E. Sheehan, and C. M. Lieber, Science **277**, 1971-1974 (1997).
- ⁵ M.-F. Yu, O. Lourie, M. J. Dyer, K. Moloni, T. F. Kelly, and R. S. Ruoff, Science **287**, 637-640 (2000).
- ⁶ M. Yu, B. Files, S. Arepalli, and R. Ruoff, Physical Review Letters **84**, 5552-5555 (2000).
- ⁷ D. H. Robertson, D. W. Brenner, and J. W. Mintmire, Physical Review B **45**, 45-48 (1992).
- ⁸ B. I. Yakobson, C. J. Brabec, and J. Bernholc, Physical Review Letters **76**, 2511-2514 (1996).
- ⁹ C. F. Cornwell and L. T. Wille, Solid State Communications **101**, 555-558 (1997).
- ¹⁰ J. P. Lu, Physical Review Letters **79**, 1297-1300 (1997).
- ¹¹ D. Troya, S. L. Mielke, and G. C. Schatz, Chemical Physics Letters **382**, 133-141 (2003).
- ¹² E. Hernandez, C. Goze, P. Bernier, and A. Rubio, Physical Review Letters **80**, 4502-4505 (1998).
- ¹³ G. VanLier, C. VanAlsenoy, V. VanDoren, and P. Geerlings, Chemical Physics Letters **326**, 181-185 (2000).
- ¹⁴ M. Arroyo and T. Belytschko, International Journal for Numerical Methods in Engineering **59**, 419-456 (2003).
- ¹⁵ N. L. Allinger, Y. H. Yuh, and J.-H. Lii, Journal of the American Chemical Society **111**, 8551-8566 (1989).
- ¹⁶ D. W. Brenner, O. A. Shenderova, J. A. Harrison, S. J. Stuart, B. Ni, and S. B. Sinnott, Journal of Physics **14**, 783-802 (2002).
- ¹⁷ C. Q. Ru, Journal of Applied Physics **87**, 7227-7231 (2000).